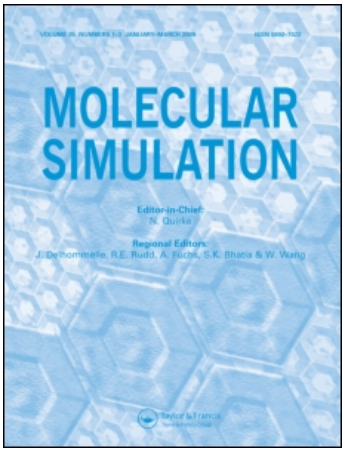

Molecular Simulation
Publication details, including instructions for authors and subscription information:
http://www.informaworld.com/smpp/title~content=t713644482

Cobalt complex based on cyclam for reversible binding of nitric oxide

O. Siri[a]; A. Tabard[b]; P. Pullumbi[c]; R. Guilard[b]
[a] Centre Interdisciplinaire de Nanoscience de Marseille (CINaM), UPR CNRS 3118, Campus de Luminy, case 913, 13288, Marseille Cedex 09, France [b] Institut de Chimie Moléculaire de l'Université de Bourgogne (ICMUB), UMR CNRS 5260, Dijon Cedex, France [c] Air Liquide, Centre de Recherche Claude-Delorme, Jouy-en-Josas Cedex, France

To cite this Article Siri, O. , Tabard, A. , Pullumbi, P. and Guilard, R.(2008) 'Cobalt complex based on cyclam for reversible binding of nitric oxide', Molecular Simulation, 34: 10, 909 — 921
To link to this Article: DOI: 10.1080/08927020802235680
URL: http://dx.doi.org/10.1080/08927020802235680

Molecular Simulation
Vol. 34, Nos. 10–15, September–December 2008, 909–921

Taylor & Francis
Taylor & Francis Group

Cobalt complex based on cyclam for reversible binding of nitric oxide

O. Siri[a], A. Tabard[b], P. Pullumbi[c]* and R. Guilard[b]*

[a]*Centre Interdisciplinaire de Nanoscience de Marseille (CINaM), UPR CNRS 3118, Campus de Luminy, case 913, 13288, Marseille Cedex 09, France;* [b]*Institut de Chimie Moléculaire de l'Université de Bourgogne (ICMUB), UMR CNRS 5260, Dijon Cedex, France;* [c]*Air Liquide, Centre de Recherche Claude-Delorme, Jouy-en-Josas Cedex, France*

(*Received 31 January 2008; final version received 29 May 2008*)

We report the synthesis and theoretical calculations of nitrosyl cobalt complexes based on saturated tetraazamacrocycle for the reversible binding of nitric oxide (NO). Density-functional theory provides a rigorous theoretical framework for analysing, interpreting and investigating important parameters in order to further tune the properties of these complexes to the target application. We focus on understanding the stability of complexes in methanol solution as well as their reactivity and stability evolution in the presence of NO, O_2 and higher nitrogen oxides intermediates. Calculations have been used to explore appropriate combinations of different macrocycles, metal centres and ligands that could be used for efficient NO release.

Keywords: nitric oxide; coordination chemistry; cobalt complexes; infrared spectroscopy; molecular modelling

1. Introduction

Nitric oxide (NO) being an endogeneous reactive molecule that plays important physiological roles in living organisms [1], its delivery to specific targets receives a great deal of attention through the study of numerous biological processes and therapeutic applications. Only a limited number of exogeneous NO-donors are available for clinical use, so the development of molecules that can release NO is of considerable interest [2]. The simplest case uses direct inhalation of NO [3] but its clinical use as a gas is technically difficult to administer [4]. Most exogeneous NO-donors are organic molecules such as nitrates which do not directly release NO owing to the biotransformations that are initially required [5–7]. More recently, the use of metal nitrosyl complexes appeared very attractive since the only direct NO-releasing drug clinically available in the US is sodium nitroprusside (iron complex) for which five toxic cyanide ions are released for every NO molecule [8,9]. Different NO-donor complexes based on ruthenium [10], iron [11–14], manganese [15] and cobalt [11,16,17] are described in the literature. Among the most promising cobalt complexes, nitrosyl cobinamide, a structural analogue of vitamin B12 (*unsaturated* cyclic tetraamine), is an efficient direct NO-releasing agent [16]. To the best of our knowledge, the use of cobalt(II) derivatives based on *saturated* cyclic polyamines such as cyclam **1** has not been reported, whereas their flexibility might allow distinct configurations of the nitrosyl complexes with specific properties [18].

Herein, we report the synthesis and theoretical studies of a cobalt(II) complex based on **1** for reversible binding of NO.

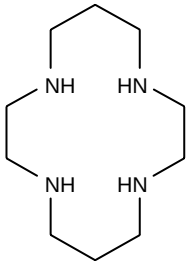

1

2. Syntheses and experimental characterisation

Cyclam **1** is a well-known, macrocyclic tetramine possessing a 14-membered ring able to form stable complexes with many metal ions [19]. The complex [(**1**)$CoCl_2$] was first synthesised by adding a solution of 0.15 mmol of **1** in dry methanol 0.15 mmol of $CoCl_2{\cdot}6H_2O$ under argon atmosphere. This reaction, when carried out under reflux for 1 h led to precipitation of [**1**-Co(III)Cl_2]Cl as bright green crystals corresponding to the oxidation of Co(II) in Co(III) as reported in [20,21].

The fresh solution of [(**1**)$CoCl_2$] was then treated with NO gas bubbled through by means of a gastight glass syringe, connected to a flow meter, equipped with a needle valve for the adjustment of the gas flow rate and calibrated between 5 and 30 ml/min. The NO gas injection effectuated at room temperature and at an absolute pressure of about 0.9 bars for 60 s time intervals lead to a rapid colour change consistent

*Corresponding authors. Emails: pluton.pullumbi@airliquide.com; roger.guilard@u-bourgogne.fr

ISSN 0892-7022 print/ISSN 1029-0435 online

DOI: 10.1080/08927020802235680
http://www.informaworld.com

with the formation of the nitrosyl complex. [(**1**)Co(NO)(Cl)]PF_6 was isolated after precipitation with $N(Bu)_4{\cdot}PF_6$ as a green solid (89% yield). Calculated composition for $C_{10}H_{24}N_5CoOCl{\cdot}PF_6$:C% 25.6; H% 5.2; N% 14.9; Cl% 7.5; F% 24.3; Co% 12.5; P% 6.6. Found composition for $C_{10}H_{24}N_5CoOCl{\cdot}PF_6$: C% 25.5; H% 5.2; N% 14.4; Cl% 7.3; F% 23.5; Co% 11.8; P% 6.2. Its infrared spectrum (KBr disk) exhibited a strong sharp absorption at 1610 cm^{-1} corresponding to the NO stretching.

This reaction can be monitored by Electron Paramagnetic Resonance (EPR) spectroscopy since the paramagnetic Co(II) species becomes diamagnetic upon coordination of NO and formation of the *trans*-[(**1**)Co(NO)(Cl)]Cl compound. The nitrosyl complex could be more easily isolated after anion exchange with $N(Bu)_4{\cdot}PF_6$ which led to the precipitation of the *trans*-[(**1**)Co(NO)(Cl)]PF_6 salt which was characterised. The *trans* configuration of the complex and the geometry of the CoNO moiety were determined by infrared spectroscopy. NO can form two distinct terminal bonding modes which have different geometries, i.e. linear and bent [22], and the most distinctive physical property is the infrared ν(NO) band for which the frequencies of bent CoNO groups are usually lower than those of linear Metal-Nitric Oxide (MNO) groups [23]. The infrared spectrum of [(**1**)Co(NO)(Cl)]Cl in 1600–1900 cm^{-1} showed one intense band at 1610 cm^{-1} which is consistent with a bent geometry. In addition, the 800–900 cm^{-1} range which gives information about the coordination scheme of the central metal ion [24] revealed three bands in agreement with the *trans* configuration. Complex *trans*-[(**1**)Co(NO)(Cl)]Cl is stable under inert atmosphere in a methanolic solution, i.e. argon bubbling did not lead to the release of NO. In contrast, such a compound is unstable in the presence of dioxygen and converted into the Co(III)–nitro complex for which the IR spectrum of the obtained complex did not show the NO vibrations but the presence of two new bands at 1355 and 828 cm^{-1} characteristic of the coordinated NO_2 group.

Interestingly, we noted that related cobalt(II) species can be five-coordinated in solution [23,25] owing to a strong *trans* influence. The *trans* influence of a ligand is defined as the extent to which that ligand weakens the bond *trans* to itself. In the *trans*-[(**1**)Co(NO)(Cl)]Cl complex for which the Co—N—O moiety is bent, NO is formally NO^- reflecting no back-bonding. This assignment is consistent with a strong trans labilizing effect as already observed for Co—NO analogues with a bent nitrosyl group. However, in the case of *trans*-[(**1**)Co(NO)(Cl)]Cl, the axial ligand Cl is not trans director to NO so that no release of NO was observed.

3. Computational methods and calculations

The structures of all of the reactants, complexes, transition states, intermediates and products were fully optimised using the Dmol^3 density-functional theory (DFT) [26,27] code as implemented in the Materials Studio® distribution of Accelrys© software package. The non-local gradient-corrected functional VWN-BP has been used for all the Dmol^3 calculations together with the double numerical plus polarisation (DNP) basis sets and the fine numerical integration grid. For all the species, the Dmol^3 calculations have been performed using the semi-core, pseudopotential option in gas as well as in the solvated phase. The hardness-conserving, semi-core pseudopotentials, called density-functional, semi-core pseudopotentials, are generated by fitting all-electron relativistic DFT results and have a non-local contribution for each channel up to $l = 2$, as well as a non-local contribution to account for higher channels. The harmonic vibrational frequencies were calculated at the same level, in order to characterise the nature of the local minima with no imaginary frequency, and those of transition states with only one imaginary frequency. The conductor-like screening model (COSMO) [28,29] model was used to model the solute molecule forming a cavity within the dielectric continuum with the permittivity representing the solvent that in our case was methanol. The direct incorporation of the solvent effects within the self consistent field procedure is a major computational advantage of the COSMO scheme. The Dmol^3/COSMO orbitals are obtained using the variational scheme enabling the derivation of accurate analytic gradients with respect to the coordinates of the solute atoms. The solvation energies depend on the choice of Dmol^3 parameters, such as the type of DFT functional, the basis set and integration grid. Recent publications [30] indicate that the Dmol^3/COSMO calculations with the VWN-BP functional can predict solvation energies with an accuracy of the order of 2 kcal/mol. Recently, we have reported the use of the semiempiric PM3-tm method, incorporating the parametrization of transition metals to the original PM3 [31,32], as implemented in the SPARTAN™ package [33] for the study of the structures and stabilities of Fe(**1**)(NO)(Cl) complexes [18]. In the present study, due to the relatively large size of the [Co(**1**)]NO complexes we have applied the same method (PM3-tm) to generate the initial stable geometries that were further optimised using Dmol^3 and we have obtained the results for the gas-phase isolated complexes as well as for their respective solvated form through Dmol^3/COSMO calculations. In order to validate and compare the PM3-tm and Dmol^3 methods for Co(**1**) complexes, the *trans*-[Co(**1**)Cl_2] was optimised with both methods and the obtained structures were compared by overlay [34] to the experimental (X-ray diffraction) data reported for this compound [20]. The accordance between the calculated PM3 and Dmol^3 and the experimental geometric parameters is quite good, the root-mean square deviation being equal to 0.101 Å (PM3) and 0.051 Å (Dmol^3).

As there could be *a priori* two oxidation states for cobalt in the complex form, and because of the recent interest in model biological systems such as vitamin B12 or isoelectronic systems with Fe(II) complexes, systematic calculations of **1**-Co(III) complexes have been carried out in parallel with those of **1**-Co(II) ones including all combinations of the axial ligands (NO, NO_2, NO_2^- and Cl^-) that could coordinate to both **1**-Co(II) or **1**-Co(III). These different cases are reported in Table 1. The different configurations of the *trans*-[Co(**1**)] complexes are specified by two numbers, the first one (Roman-in parentheses) stands for the oxidation state of cobalt while the second one indicates the partial charge of the cobalt-containing half-complex. The total charge of the complex is reported in Table 1.

The different calculations carried out in this study are reported in Table 2. Each complex has been calculated in gas phase (empty) and in solvent (methanol) using the COSMO method to include solvent effects.

In Table 3, the stabilities of **1**-Co(II) and **1**-Co(III) complexes are reported for both gas phase and in the methanol species. It appears clear from this table that the **1**-Co(II) complexes are much more stable than the **1**-Co(III) ones as would normally be expected due to the extra electron. However, the difference is reduced when the solvent effect is taken into account. In our further analysis of the chemical reactivity and stability of **1**-cobalt complexes, we will focus only on **1**-Co(II) ones.

The highest occupied molecular orbital (HOMO) and the lowest unoccupied molecular orbital (LUMO) of a species are known as frontier molecular orbitals (FMO) after Fukui's work [35] on their role in predicting chemical reactivity. It has been shown that these orbitals play a major role in governing many chemical reactions and determining electronic band gaps in organometallic complexes and solids; they are also responsible for the formation of many charge transfer complexes [36]. According to the FMO theory of chemical reactivity, the formation of a transition state is due to the interaction between the frontier orbitals (HOMO and LUMO) of the reacting species [35,36]. The energy of the HOMO is directly related to the ionisation potential and characterises the reactivity of the molecule towards an electrophilic reaction. The energy of the LUMO is directly linked to the electron affinity and characterises the susceptibility of the molecule towards an attack by nucleophiles. Moreover, a large HOMO–LUMO gap corresponds to a high stability for the molecule but to a lower reactivity [37,38].

Another useful approach in predicting the reactivity of species, involving a single pair of frontier orbitals, is the Hard–Soft Acid Base principle introduced by Pearson [39–42] and developed in the framework of DFT by Parr [43–45]. Following the definition of Pearson [39–41] of global hardness (GH) (η), and global softness (GS) (S) based upon the finite difference approximation, we have calculated the GH as: $\eta = 1/2\ (\varepsilon_{LUMO} - \varepsilon_{HOMO})$; and the GS as: $S = 1/\eta$. In Table 4, we have reported the values of GH and GS for all [**1**-Co(II)]-L_iL_j where L_i and L_j are two ligands from (NO, NO_2, NO_2^- and Cl^-). GS has been formally connected with molecular polarizability.

In Table 5, we report the calculations carried out for the isolated ligands (Cl^-, NO, NO_2 and NO_2^-) in gas phase and in methanol, including NO stretching vibration frequencies that compare well with experimental observations. In Table 6, we report the strength of [L_i-**1**-Co(II)] – L_j bond where L_i and L_j are two ligands from (NO, NO_2, NO_2^- and Cl^-) in gas phase and in methanol solvent.

In Table 7, we report the calculated NO vibrational stretching frequencies (cm^{-1}) for different [L_i-**1**-Co(II)]-L_j complexes where L_i and L_j are two ligands from (NO, NO_2, NO_2^- and Cl^-). The accuracy of the vibrational frequency calculations is a function of the theoretical method used. In many cases, the experimentally measured values differ significantly from those calculated theoretically. One source of discrepancy is that the experimental values are often determined in solution or in a solid matrix, while calculated values refer to the gas phase. Quite good results can be obtained from density-functional calculations using gradient-corrected functionals.

Table 1. Total charge of **1**-Co(II) and **1**-Co(III) calculated complexes with selected axial ligands (NO, NO_2, NO_2 and Cl^-).

	Ligands			
Complexes	NO	NO_2	NO_2^-	Cl^-
[**1**-Co(II)-Cl]$^+$	1	1	0	0
[**1**-Co(III)-Cl]$^{2+}$	2	2	1	1
[**1**-Co(II)-NO]$^{2+}$	2	2	1	1
[**1**-Co(III)-NO]$^{3+}$	3	3	2	2
[**1**-Co(II)-NO_2]$^+$	1	1	0	0
[**1**-Co(III)-NO_2]$^{2+}$	2	2	1	1
[**1**-Co(III)-NO_2]$^{3+}$	3	3	2	2

4. Discussion

In our combined experimental–theoretical approach, DFT calculations were used to help understand NO competitive coordination to **1**-cobalt complexes in methanol solution in presence of other ligands (O_2, NO_2, NO_2^- and Cl^-). Systematic calculations of all possible combinations of cobalt oxidation state and the two *trans*-coordinating ligands have been undertaken for the isolated structures (35 [**1**-Co(II)]-L_iL_j structures, where L_i and L_j are two ligands from (NO, NO_2, NO_2^- and Cl^-)) and their analogues in methanol counterparts. The results of such calculations reported in Table 2 indicate that the solvent effect has an important role on the stability of these complexes. The comparative analysis of the stability of Co(II) complexes with their Co(III) analogue structures, reported in Table 3, clearly indicates that Co(II) complexes are more stable due to the electron

Table 2. Energies for the gas phase and methanol complexes of **1**-Co(II) or **1**-Co(III) with different ligands.

		NO	NO_2	NO_2^-	Cl^{-1}
*[**1**-Co(II)-Cl]$^+$*					
Complex charges	1	1	1	0	0
In gas phase (au)	−1241.893521	−1371.921846	−1447.179030	−1447.338003	−1702.381070
In methanol (au)	−1242.013279	−1372.001621	−1447.259219	−1447.376739	−1702.438684
Solvent effect (kcal/mol)	−75.15	−50.06	−50.32	−24.31	−36.15
HOMO (eV) gas phase	−7.78	−7.85	−9.38	−2.61	−1.36
LUMO (eV) gas phase	−6.08	−6.67	−6.15	−1.56	−0.79
HOMO–LUMO (eV) gas phase	1.70	1.18	3.23	1.05	0.57
HOMO (eV) in methanol	−4.11	−5.05	−6.64	−3.50	−3.50
LUMO (eV) in methanol	−1.92	−3.74	−3.23	−2.08	−1.95
HOMO–LUMO (eV) in methanol	2.19	1.31	3.40	1.42	1.56
*[**1**-Co(III)-Cl]$^{+2}$*					
Charges	2	2	2	1	1
In gas phase (au)	−1241.567820	−1371.552237	−1446.754605	−1447.179030	−1702.261573
In methanol (au)	−1241.854823	−1371.802123	−1447.002374	−1447.259219	−1702.315769
Solvent effect (kcal/mol)	−180.10	−156.81	−155.48	−50.32	−34.01
HOMO (eV) gas phase	−13.62	−13.20	−14.04	−9.38	−8.65
LUMO (eV) gas phase	−11.91	−12.14	−13.59	−6.15	−5.83
HOMO–LUMO (eV) gas phase	1.71	1.05	0.45	3.23	2.82
HOMO (eV) in methanol	−7.14	−6.89	−7.87	−6.64	−6.41
LUMO (eV) in methanol	−4.66	−5.83	−7.42	−3.23	−3.50
HOMO–LUMO (eV) in methanol	2.48	1.07	0.45	3.40	2.91
*[**1**-Co(II)-NO]$^{+2}$*					
Charges	2	2	2	1	1
In gas phase (au)	−911.295746	−1041.256722	−1116.490312	−1116.853893	−1371.921846
In methanol (au)	−911.556231	−1041.512176	−1116.742836	−1116.938316	−1372.001621
Solvent effect (kcal/mol)	−163.46	−160.30	−158.46	−52.98	−50.06
HOMO (eV) gas phase	−12.65	−11.90	−12.95	−7.72	−7.85
LUMO (eV) gas phase	−10.87	−11.31	−12.09	−6.84	−6.67
HOMO–LUMO (eV) gas phase	1.78	0.60	0.86	0.88	1.18
HOMO (eV) in methanol	−5.89	−6.64	−6.74	−4.91	−5.05
LUMO (eV) in methanol	−4.14	−5.10	−5.78	−3.84	−3.74
HOMO–LUMO (eV) in methanol	1.75	1.55	0.97	1.07	1.31
*[**1**-Co(III)-NO]$^{+3}$*					
Charges	3	3	3	2	2
In gas phase (au)	−910.747861	−1040.732515	−1115.941179	−1116.490312	−1371.552237
In methanol (au)	−911.316027	−1041.27666	−1116.489015	−1116.742836	−1371.802123
Solvent effect (kcal/mol)	−356.53	−341.46	−343.77	−158.46	−156.81
HOMO (eV) gas phase	−18.28	−17.69	−18.16	−12.95	−13.20
LUMO (eV) gas phase	−16.79	−16.52	−16.80	−12.09	−12.14
HOMO–LUMO (eV) gas phase	1.49	1.17	1.36	0.86	1.05
HOMO (eV) in methanol	−8.17	−8.02	−8.76	−6.74	−6.89
LUMO (eV) in methanol	−6.99	−6.80	−7.20	−5.78	−5.83
HOMO–LUMO (eV) in methanol	1.56	1.56	1.56	0.97	1.07
*[**1**-Co(II)-NO_2]$^+$*					
Charges	1	1	1	0	0
In gas phase (au)	−986.854343	−1116.853893	−1192.117753	−1192.287363	−1447.338003
In methanol (au)	−986.947275	−1116.938316	−1192.202831	−1192.323930	−1447.376739
Solvent effect (kcal/mol)	−58.32	−52.98	−53.39	−22.94	−24.31
HOMO (eV) gas phase	−6.80	−7.72	−9.05	−4.62	−2.61
LUMO (eV) gas phase	−5.34	−6.84	−6.21	−1.73	−1.56
HOMO–LUMO (eV) gas phase	1.46	0.88	2.84	2.89	1.05
HOMO (eV) in methanol	−3.80	−4.91	−6.40	−5.2	−3.50
LUMO (eV) in methanol	−2.28	−3.84	−3.21	−2.2	−2.08
HOMO–LUMO (eV) in methanol	1.53	1.07	3.19	2.98	1.42
*[**1**-Co(III)-NO_2]$^{+2}$*					
Charges	2	2	2	1	1
In gas phase (au)	−986.520493	−1116.490312	−1191.703220	−1192.117753	−1447.179030
In methanol (au)	−986.798345	−1116.742836	−1191.950985	−1192.202831	−1447.259219

Table 2 – *continued*

		NO	NO_2	NO_2^-	Cl^{-1}
Solvent effect (kcal/mol)	−174.35	−158.46	−155.48	−53.39	−50.32
HOMO (eV) gas phase	−13.98	−12.95	−14.12	−9.05	−9.38
LUMO (eV) gas phase	−11.33	−12.09	−13.48	−6.21	−6.15
HOMO–LUMO (eV) gas phase	2.65	0.86	0.64	2.84	3.23
HOMO (eV) in methanol	−7.51	−6.74	−7.98	−6.40	−6.64
LUMO (eV) in methanol	−4.44	−5.78	−7.41	−3.21	−3.23
HOMO–LUMO (eV) in methanol	3.07	0.97	0.58	3.19	3.40
*[**1**-Co(III)-NO_2]$^{+3}$*					
Charges	3	3	3	2	2
In gas phase (au)	−985.932523	−1115.941179	−1191.111532	−1191.703220	−1446.754605
In methanol (au)	−986.503361	−1116.489015	−1191.657260	−1191.950985	−1447.002374
Solvent effect (kcal/mol)	−358.21	−343.77	−342.45	−155.48	−155.48
HOMO (eV) gas phase	−18.56	−18.16	−19.31	−14.12	−14.04
LUMO (eV) gas phase	−17.64	−16.80	−18.20	−13.48	−13.59
HOMO–LUMO (eV) gas phase	0.92	1.36	1.16	0.64	0.45
HOMO (eV) in methanol	−8.87	−8.76	−9.97	−7.98	−7.87
LUMO (eV) in methanol	−8.13	−7.20	−8.82	−7.41	−7.42
HOMO–LUMO (eV) in methanol	0.74	1.56	1.17	0.58	0.45
*[**1**-Co(III)]$^{+3}$*					
Charges	3	3	3	2	2
In gas phase (au)	−780.705952	−910.747861	−985.932523	−986.520493	−1241.567820
In methanol (au)	−781.356894	−911.316027	−986.503361	−986.798345	−1241.854823
Solvent effect (kcal/mol)	−408.47	−356.53	−358.21	−174.35	−180.10
HOMO (eV) gas phase	−18.82	−18.28	−18.56	−13.98	−13.62
LUMO (eV) gas phase	−18.43	−16.79	−17.64	−11.33	−11.91
HOMO–LUMO (eV) gas phase	0.39	1.49	0.92	2.65	1.71
HOMO (eV) in methanol	−8.49	−8.17	−8.87	−7.51	−7.14
LUMO (eV) in methanol	−6.71	−6.99	−8.13	−4.44	−4.66
HOMO–LUMO (eV) in methanol	1.78	1.18	0.74	3.07	2.48
*[**1**-Co(II)]$^{+2}$*					
Charges	2	2	2	1	1
In gas phase (au)	−781.294661	−911.295746	−986.520493	−986.854343	−1241.893521
In methanol (au)	−781.573470	−911.556231	−986.798345	−986.947275	−1242.013279
Solvent effect (kcal/mol)	−174.96	−163.46	−174.35	−58.32	−75.15
HOMO (eV) gas phase	−13.46	−12.65	−13.98	−6.80	−7.78
LUMO (eV) gas phase	−11.41	−10.87	−11.33	−5.34	−6.08
HOMO–LUMO (eV) gas phase	2.06	1.78	2.65	1.46	1.70
HOMO (eV) in methanol	−5.04	−5.89	−7.51	−3.80	−4.11
LUMO (eV) in methanol	−2.53	−4.14	−4.44	−2.28	−1.92
HOMO–LUMO (eV) in methanol	2.51	1.75	3.07	1.53	2.19

Table 3. Relative stability (kcal/mol) of **1**-[Co(II)/Co(III)] complexes in gas phase and methanol.

Co(II)–Co(III) complexes		NO	NO_2	NO_2^-	Cl^{-1}
[**1**-Co(II)–**1**-CO(III)]Cl	In gas phase	−231.93	−266.33	−99.76	−74.99
	In methanol	−125.19	−161.17	−73.74	−77.13
[**1**-Co(II)–**1**-CO(III)NO	In gas phase	−328.95	−344.59	−228.15	−240.88
	In methanol	−147.79	−159.28	−122.67	−125.19
[**1**-Co(II)–**1**-CO(III)]NO_2_a	In gas phase	−228.15	−260.12	−106.43	−99.76
	In methanol	−122.67	−158.04	−75.99	−73.74
[**1**-Co(II)–**1**-CO(III)]NO_2_b	In gas phase	−572.74	−631.41	−366.56	−366.09
	In methanol	−281.94	−342.35	−234.03	−234.92
[**1**-Co(II)–**1**-CO(III)]	In gas phase	−343.80	−368.96	−209.49	−204.38
	In methanol	−150.73	−185.11	−93.46	−99.43

Table 4. Global hardness (GH) and global softness (GS) for **1**-Co(II) complexes in gas phase and methanol.

GH in (eV) and GS in (1/eV)			NO	NO_2	NO_2^{-1}	Cl^{-1}
[**1**-Co(II)-Cl]$^{+1}$	In gas phase GH	0.85	0.59	1.61	0.53	0.29
	In gas phase GS	1.18	1.69	0.62	1.90	3.50
	In methanol GH	1.10	0.66	1.70	0.71	0.78
	In methanol GS	0.91	1.53	0.59	1.41	0.97
[**1**-Co(II)-NO]$^{+2}$	In gas phase GH	0.89	0.30	0.43	0.44	0.59
	In gas phase GS	1.12	3.36	2.34	2.28	1.69
	In methanol GH	0.87	0.77	0.48	0.54	0.66
	In methanol GS	1.15	1.29	2.07	1.86	1.53
[**1**-Co(II)-NO_2]$^{+1}$	In gas phase GH	0.73	0.44	1.42	1.44	0.53
	In gas phase GS	1.37	2.28	0.70	0.69	1.90
	In methanol GH	0.76	0.54	1.60	1.49	0.71
	In methanol GS	1.31	1.86	0.63	0.67	1.41
[**1**-Co(II)]$^{+2}$	In gas phase GH	1.03	0.89	1.33	0.73	0.85
	In gas phase GS	0.97	1.12	0.75	1.37	1.18
	In methanol GH	3.79	5.02	5.97	3.04	3.02
	In methanol GS	0.26	0.20	0.17	0.33	0.33

imbalance of the Co(III) species than that which is observed experimentally when compensated by an anion species. The electrostatic interaction between the two charged species would normally stabilise the Co(III) complex. When the effect of the solvent is taken into account, the difference in stability between calculated **1**-Co(II) and **1**-Co(III) complexes is reduced.

In Table 4, the global stability (GH) and reactivity (GS) indices are reported for **1**-Co(II)-L_iL_j complexes where L_i and L_j are two ligands from NO, NO_2, NO_2^- or Cl^-. According to the principle of maximum hardness [43], the more stable complexes should have maximum hardness value. The calculated GH values for each complex in the gas phase or methanol, reported in Table 6 indicate that between the calculated complexes **1**-Co(II)-L_iL_j the [**1**-Co(II)-$ClNO_2$]$^+$, [**1**-Co(II)-$(NO_2)_2$]$^+$ and **1**-Co(II)-$(NO_2)_2$]$^+$ are the most stable ones. The reported values of GS for the same complexes also indicate that the most reactive complexes are [**1**-Co(II)-ClNO]$^+$, [**1**-Co(II)-$NONO_2$]$^{+2}$ and [**1**-Co(II)-$NONO_2$]$^+$. Table 5 shows the calculated properties of the considered ligands (NO, NO_2, NO_2^- and Cl^-). It appears clear that the most stable ligand is the anion Cl^- and the most reactive one is the NO_2 radical. In this table, we also report the vibrational frequencies of the isolated ligands that will be further discussed when the IR spectra of the complexes are compared to experimental ones.

In Figure 1, we report the optimised structures of all stable complexes [**1**-Co(II)]-L_iL_j, where L_i and L_j are two ligands from (NO, NO_2, NO_2^- and Cl^-), reported in Table 6. The analysis of the interaction of **1**-Co(II)-Cl_2 with the NO reported in this table confirms the experimental finding that the formation of the trans Cl—Co—NO cyclam complex is observed at low NO concentrations and in the absence

Table 5. Calculated properties of ligands in gas phase and methanol.

Ligands	NO	NO_2	NO_2^{-1}	Cl^{-1}
Charge	0	0	−1	−1
Energy (au) in gas phase	−129.942283	−205.179536	−205.23013	−460.27953
Energy (au) in methanol	−129.942667	−205.181183	−205.30483	−460.400715
Solvent effect (kcal/mol)	−0.24	−1.03	−46.87	−76.04
HOMO gas phase (eV)	−12.13	−9.25	1.44	1.93
LUMO gas phase (eV)	−5.43	−7.4	4.18	16.32
HOMO−LUMO gap_g	6.7	1.85	2.74	14.39
GH gas phase (eV)	3.35	0.93	1.37	7.2
GS gas phase (1/eV)	0.3	1.08	0.73	0.14
HOMO methanol (eV)	−10.97	−6.36	−1.93	−4.72
LUMO methanol (eV)	−4.29	−4.85	0.15	9.7
HOMO−LUMO gap_m	6.68	1.51	2.08	14.42
GH methanol (eV)	3.34	0.75	1.04	7.21
GS methanol (1/eV)	0.3	1.33	0.96	0.14
NO stretching (cm^{-1}) asym	1893	1628	1207	
NO stretching (cm^{-1}) sym		1329	1307	
NO stretching exp (cm^{-1}) asym	1904	1618		
NO stretching exp (cm^{-1}) sym		1318		

Table 6. Complex–ligand bond energies (kcal/mol) in gas phase and methanol.

Complex		Ligands			
		NO	NO_2	NO_2^{-1}	Cl^{-1}
[**1**-Co(II)-Cl]$^{+1}$	In gas phase	−54.0	−66.5	−134.5	−130.5
	In methanol	−28.7	−40.6	−36.8	−15.5
[**1**-Co(II)-NO]$^{+2}$	In gas phase	−11.7	−9.4	−205.8	−217.5
	In methanol	−8.3	−3.4	−48.5	−28.0
[**1**-Co(II)-NO_2]$^{+1}$	In gas phase	−35.9	−52.6	−127.3	−128.1
	In methanol	−30.4	−46.7	−45.1	−18.0
[**1**-Co(II)]$^{+2}$	In gas phase	−36.9	−29.1	−206.8	−200.4
	In methanol	−25.2	−27.4	−43.3	−24.5

of oxygen. As a matter of fact, the calculated Co—NO bond energy (28.7 kcal/mol) is nearly the double of the Co—Cl one (15.5 kcal/mol). It should be noted, however, that in this analysis only the calculations which take into account the solvent effects should be considered. These results are well correlated with the GH data reported in Table 4. If we consider the replacement of the second Cl^- by a NO ligand and the formation of a trans NO—Co—NO cyclam complex, the predicted binding energy of the second NO to Co is of only 8.3 kcal/mol which is nearly half of the corresponding Cl—Co binding energy (15.5 kcal/mol). This prediction perfectly fits with the experimental observations. The formation of the trans NO—Co—NO cyclam complex has not been observed experimentally. Following the analysis of the stability of the complexes reported in Table 6, we can say that the binding of the [**1**-Co(II)]$^{2+}$ complex with the NO ligand in methanol (25.2 kcal/mol) is nearly the same as its binding with the Cl^- ligand (24.5 kcal/mol) and adding a trans-second ligand different from the first one is energetically favoured. A **1**-Co(II)]L_i complex will preferably form a **1**-Co(II)]-L_iL_j structure, where L_i and L_j are two ligands from (NO and Cl^-) and L_i is different from L_j.

The addition of a neutral NO_2 ligand to a methanol solution containing **1**-Co(II)-Cl_2 should favour the trans **1**-Co(II)-$ClNO_2$. As reported in Table 6, the binding energy of NO_2 on **1**-Co(II)-Cl complex is about 40.6 kcal/mol which is sensibly higher than the NO binding on the same complex. At the same time, the NO_2 binding energy to the ligand-free [**1**-Co(II)]$^{2+}$ complex in methanol (27.4 kcal/mol) is very similar to the bond energy of the NO and Cl^- ligands (25.2 and 24.5 kcal/mol, respectively) but once the [**1**-Co(II)]NO_2 half-complex is formed, binding of a second NO_2 ligand is favoured (46 kcal/mol) over NO (35.9 kcal/mol) or Cl^- (18 kcal/mol). This trend is in good agreement with the stability estimation from the GH values in Table 4. In the experiments in which dioxygen was introduced to the methanol solution containing the trans **1**-Co(II)-ClNO complex new IR bands were observed corresponding to a coordinated NO_2 group to the cobalt centre. This result confirms the theoretical predictions related to the stability of [**1**-Co(II)]L_iNO_2 complexes where L_i is a ligand from (NO, NO_2, NO_2^- and Cl^-). The predicted NO vibrational spectra of the different stable **1**-Co(II)-L_iL_j complexes, where L_i and L_j are two ligands from (NO, NO_2, NO_2^- and Cl^-) are reported in Table 7. These predictions were confirmed by the experimental analysis of the IR spectra evolution during sequential treatment of the solution containing **1**-Co(II)Cl_2 with NO, Ar and O_2 gas streams and reported in Figures 2–5. In Figure 2, the observed intense band at 1610 cm^{-1} for the **1**-Co(II)NOCl complex has been predicted in quite good agreement at 1593 cm^{-1} and the overall shape of the IR spectrum is very well

Table 7. Calculated NO stretching frequencies of different complexes.

Calculated N—O vibrational frequencies (cm^{-1})		NO	NO_2	NO_2^{-1}	Cl^{-1}
[**1**-Co(II)-Cl]$^{+1}$	NO stretching (cm^{-1}) asym	1593	1432		
	NO stretching (cm^{-1}) asym		1441	1527	
	NO stretching (cm^{-1}) sym		1309	1503	
[**1**-Co(II)-NO]$^{+2}$	NO stretching (cm^{-1}) asym	1650	1786	1671	1594
	NO stretching (cm^{-1}) asym	1738	1517	1489	
	NO stretching (cm^{-1}) sym		1293	1376	
[**1**-Co(II)-NO_2]$^{+1}$	NO stretching (cm^{-1}) asym	1671	1569	1516	1527
	NO stretching (cm^{-1}) asym	1489	1586	1518	
	NO stretching (cm^{-1}) sym	1376	1493	1263	1503
[**1**-Co(II)]$^{+2}$	NO stretching (cm^{-1}) asym	1778			
	NO stretching (cm^{-1}) asym		1618	1389	
	NO stretching (cm^{-1}) sym		1444	1237	

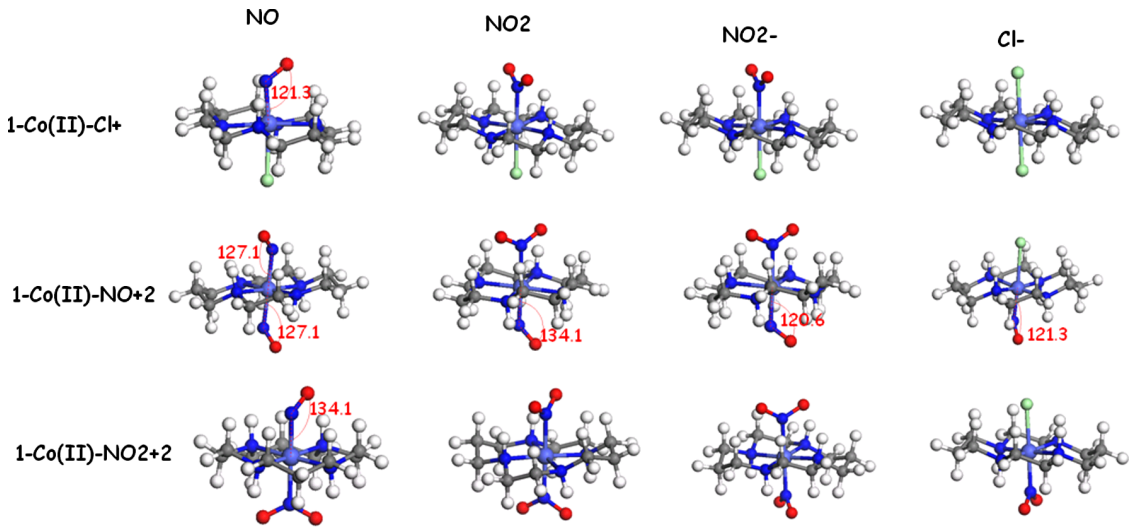

Figure 1. Optimised structures of **1**-Co(II) trans L_i, L_j complexes. L_i, L_j are ligands from (NO, NO_2, NO_2^- and Cl^-).

reproduced apart from the region around 3500 cm^{-1} corresponding to the H—O stretching of the solvent (methanol) molecules. The introduction of the oxygen in the methanol solution containing the **1**-Co(II)NOCl was followed by the presence of new NO stretching bands around 1355 cm^{-1} characteristic of coordination of NO_2. According to our calculations, these bands can be attributed either to **1**-Co(II)$ClNO_2$ (calculated around 1309 cm^{-1}) or **1**-Co(II)$NONO_2$ (predicted at 1376 cm^{-1}) or **1**-Co(II)NO_2NO_2 (predicted at 1263 cm^{-1}). In Figure 3, we reported the experimental and predicted IR spectra of [**1**-Co(II)$ClNO_2$]$^+$ and [**1**-Co(II)$ClNO_2$] species corresponding to two different (NO_2 and NO_2^-) species. From

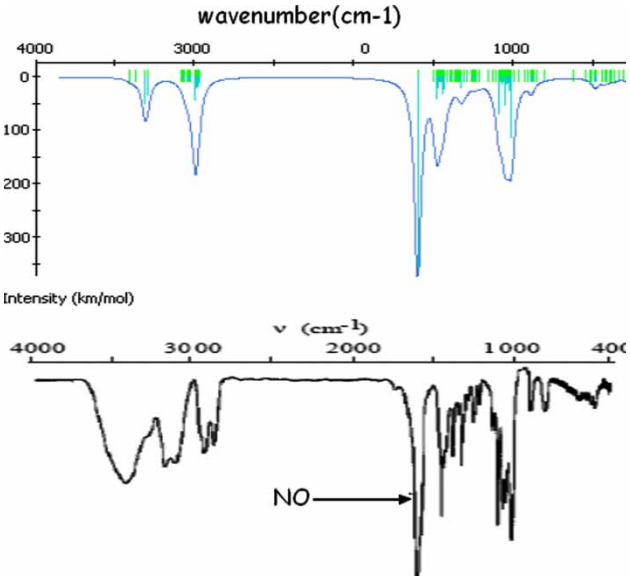

Figure 2. Experimental and simulated IR spectra of **1**-Co(II) ClNO complex.

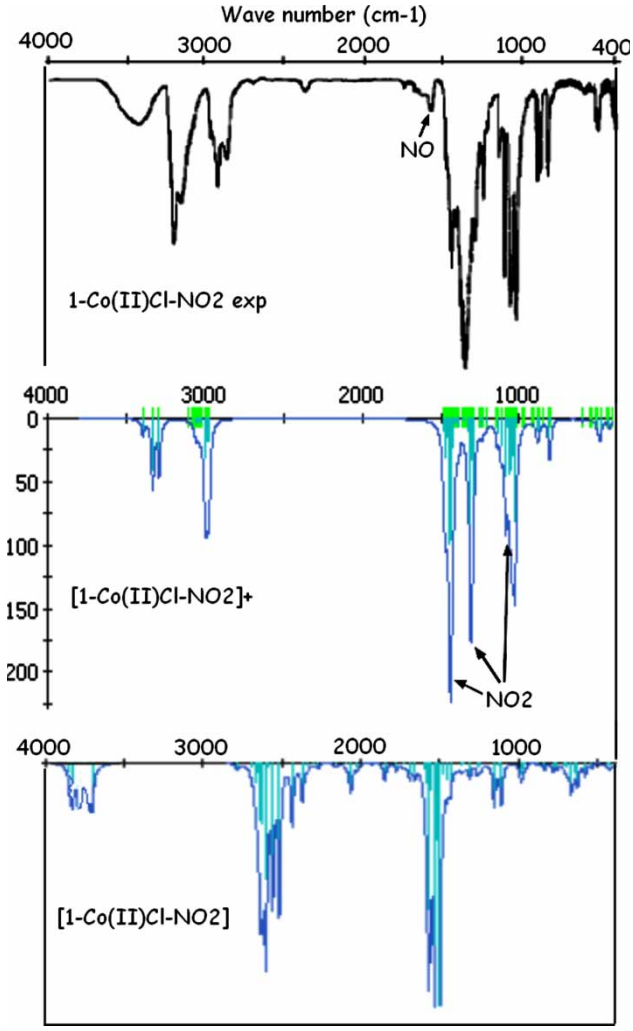

Figure 3. Experimental and simulated IR spectra of [**1**-Co(II) $ClNO_2$]$^+$ and [**1**-Co(II)$ClNO_2$] complexes.

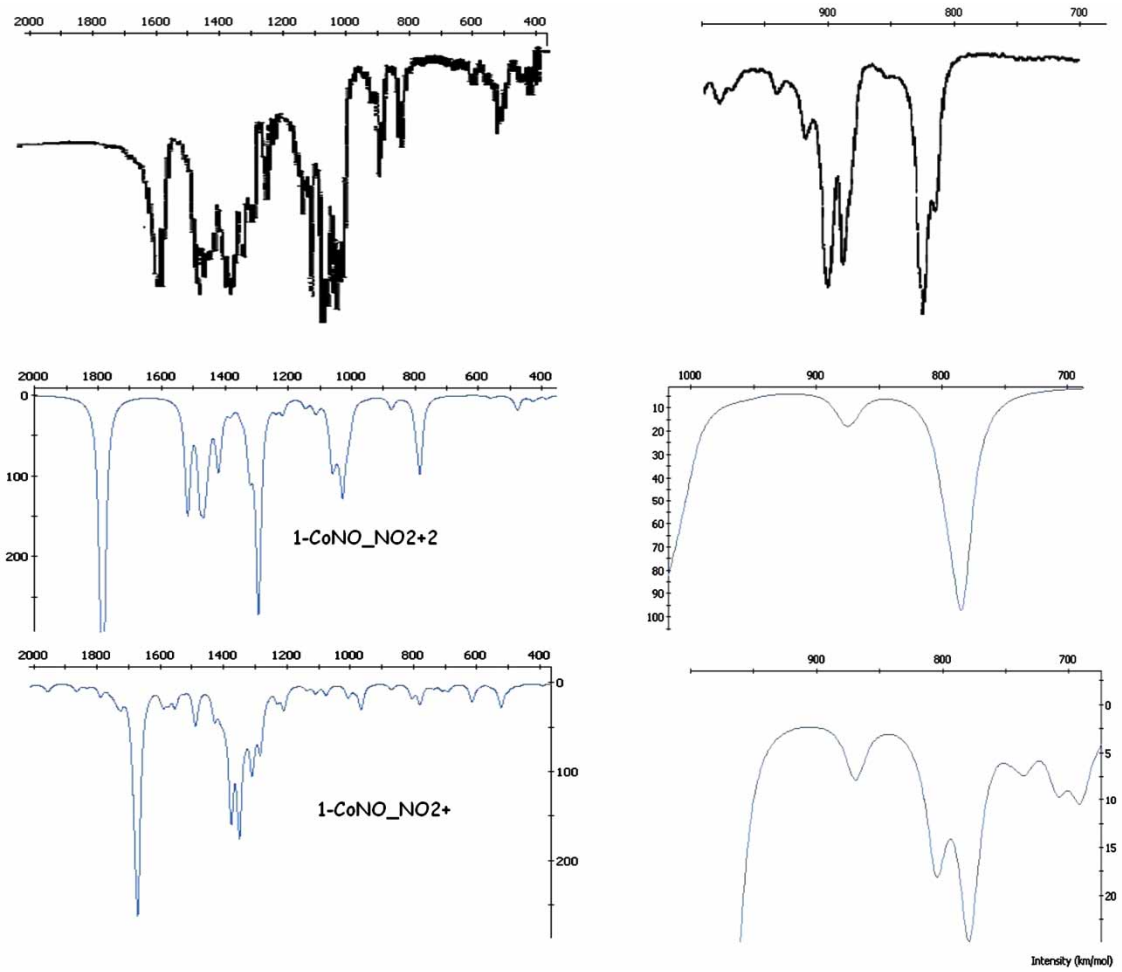

Figure 4. Experimental and simulated IR spectra of [**1**-Co(II)$NONO_2$]$^{+2}$ and [**1**-Co(II)$NONO_2$]$^{+}$ complexes.

the comparison of the overall shape of the predicted spectra, it is clear that the one observed corresponds well to the [**1**-Co(II)$ClNO_2$]$^{+}$ complex. This result is in perfect agreement with the predicted bond strength of [**1**-Co(II)$ClNO_2$]$^{+}$ complex corresponding to the coordination of NO_2 ligand on the metal centre of the [**1**-Co(II)Cl]$^{+2}$ complex.

By varying the flow rate of NO as well as the quantity and duration of dioxygen bubbling into the solution flask, a drastic evolution of the experimental spectra was observed; however, it is not evident to experimentally attribute the vibrational bands to different species due to the evolution of the axial ligands in solution.

In order to gain some insight into the evolution of the complexes, in Figures 4 and 5, the same experimental spectrum has been compared to the simulated ones of **1**-Co(II)$NONO_2$ and **1**-Co(II)NO_2NO_2.

From Figure 4, it is clear that the attribution of the observed bands is less evident than in the case of the initial complexes. This is also due to the superposition of spectra of different species present in solution. However, the trend corresponding to the similarity of the bands of experimental and simulated spectra allows us to further correlate the observed spectrum to the one corresponding to the [**1**-Co(II)$NONO_2$]$^{+}$ complex. This is supported also by the fact that the latter is much more stable in solution, as reported in Table 6.

In Figure 5, we report the comparison of the same experimental spectrum reported in Figure 4, together with the corresponding ones to [**1**-Co(II)$(NO_2)_2$]$^{+2}$ and [**1**-Co(II)$(NO_2)_2$]$^{+}$. From a rapid comparison of the aligned spectra, it is evident that the experimental one can be considered as a combination of the simulated ones with some contribution from the spectrum of [**1**-Co(II)$NONO_2$]$^{+}$ reported in Figure 4. As predicted in Table 6, all three species have similar stabilities. The analysis of the bond strength of these three complexes also suggests that **1**-Co(II)NO_2NO_2 (both species) are very stable but no direct experimental observation has been possible. Following this study, we propose a modification of the experimental conditions that would favour the isolation of these complexes.

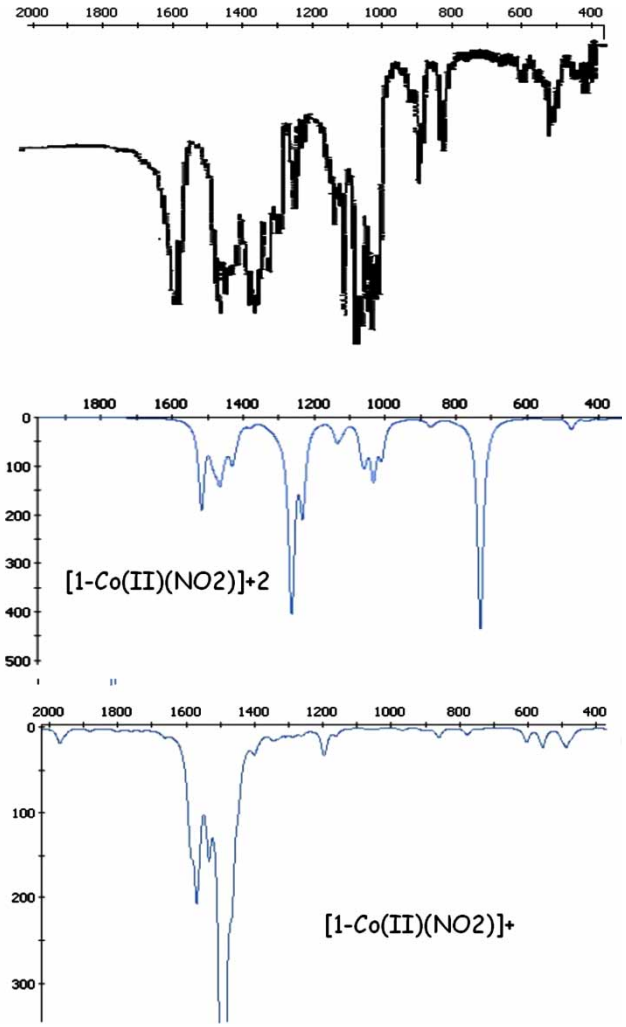

Figure 5. Experimental and simulated IR spectra of [**1**-Co(II)$(NO_2)_2]^{+2}$ and [**1**-Co(II)$(NO_2)_2]^{+}$ complexes.

In the following section, we discuss the mechanism of the formation of different predicted complexes in methanol solution starting with the oxidation of NO in the presence of dioxygen to give nitrogen dioxide; this is an important reaction which has been extremely well studied in the gas phase in relation to air pollution caused by different nitrogen oxides but whose outcome in water solution gives exclusively nitrite ions, with few nitrate ions. The mechanism of NO oxidation by dioxygen to NO_2 in gas phase has been recently [46,47] explained by the formation of the intermediate ONOONO species that undergoes homolytic O—O bond breaking. The aqueous reaction of NO with dioxygen occurs with the following overall stoichiometry:

$$4\,NO + O_2 + 2\,H_2O = 4\,H^+ + 4\,NO_2^-.$$

As a result of these reactions in methanol solution, in the presence of NO and O_2, one also finds NO_2 and NO_2^-. In order to respond to the question, whether the oxidation of the NO coordinated to **1**-Co(II), to NO_2, is catalysed by the Co(II) centre or whether NO is first oxidised in solution and is then exchanged with the Co-coordinated NO, we have undertaken calculations of the oxidations of NO in both these cases in gas phase as well as in methanol solutions. We found that, as previously reported [46,47], the first stage of NO oxidation corresponds to the formation of the ON—OO intermediate with a small barrier of 13.2 (14.5) kcal/mol in gas phase (in solution) while for the NO coordinated to the cyclam-Co(II) complex the formation of the **1**-Co(II)NO—OO showed a barrier of -0.4 (5.0) kcal/mol in gas phase (in methanol solution). This indicates that the cobalt acts as a catalyst for NO oxidation. The second step corresponds to the coordination of a second NO to the ON—OO species followed by the homolytic breaking of the O—O bond and formation of two NO_2 species. The calculation for the simple and Co-coordinated NO—OO—NO species indicated that formation of **1**-Co(II)$NO_2 +$ NO_2 species in solution is 38.62 kcal/mol more stable than the cyclam-Co(II)NO—OO—NO complex while this difference for the simple species is only 15.61 kcal/mol. This result clearly indicates that the formation of **1**-Co(II)NO_2NO_2 complex is favoured not only energetically but also based upon reactivity data.

Several hypotheses have been posed to explain nitrite formation in solutions. The electrophile–nucleophile interaction involves the overlap of the HOMO of the nucleophile with the LUMO of the electrophile to form a couple of new bonding and antibonding orbitals. The closer the energy between the two interacting orbitals, the greater is their interaction. Soft–soft interactions are mostly controlled by the frontier orbitals of the interacting systems and in the case of the hard–hard type of interactions, the contribution of electrostatic interaction becomes more significant.

It should be noticed, however, that the orbital interaction alone does not take into account the charge interaction effects (interaction between charged species) as well as the overlapping of the orbitals that is partially controlled by their respective symmetries. In Table 8, the difference energy between the HOMO of the nucleophile [**1**-Co(II)] complex and the LUMO of the electrophile ligand (Cl^-, NO, NO_2 and NO_2^-) has been reported. The overall effect of the solvent is to reduce the gap between the HOMO of the nucleophile and the LUMO of the electrophile, in agreement with the experimental observation of new species formation in methanol solutions [**1**-Co(II)]L_i in the presence of different ligands (NO, NO_2, NO_2^- and Cl^-). The differences in the HOMO–LUMO gap between the reactants reported in Table 8 for the charged ligands NO_2^- and Cl^- are compensated by the charge interaction between the **1**-Co(II) complex that bears a positive charge and the negatively charged ligands.

Table 8. Energy difference HOMO (nu) – LUMO (el) of reactants in kcal/mol.

Complexes		Ligands			
		NO	NO_2	NO_2^{-1}	Cl^{-1}
[**1**-Co(II)-Cl]$^{+1}$	In gas phase	−2.36	−0.38	−11.97	−24.11
	In methanol	0.18	0.74	−4.26	−13.81
[**1**-Co(II)-NO]$^{+2}$	In gas phase	−7.22	−5.25	−16.83	−28.97
	In methanol	−1.60	−1.04	−6.04	−15.59
[**1**-Co(II)-NO_2]$^{+1}$	In gas phase	−1.38	0.60	−10.99	−23.13
	In methanol	0.49	1.05	−3.95	−13.50
[**1**-Co(II)]$^{+2}$	In gas phase	−8.04	−6.06	−17.65	−29.79
	In methanol	−0.76	−0.19	−5.19	−14.74

It is important to note that it is not only the charge interaction between the reactants and the energy difference of their frontier orbitals which are important in explaining the reactivity of these complexes, but also the localisation of the orbitals on the reacting species. For this reason, we have calculated the Fukui functions corresponding to different electrophilic and nucleophilic attacks and have used these data to complement the reactivity information.

In Figure 6, we report the different steps of the NO coordination to the **1**-Co(II) complex followed by its oxidation and the further transformation of NO into NO_2. In this figure, we represent graphically the Fukui function indices located at the sites of nucleophilic and electrophilic attack for all the intermediaries of the reaction. The Fukui functions provide valuable information on the possible positions of reactivity and confirm the experimental observations for these complexes. As reported in Figure 2, the Fukui function for NO (electrophile) and **1**-Co(II)Cl (nucleophile) indicate that the maximum interaction is obtained between the metal centre and the Nitrogen atom of NO. The optimised structure obtained from the interaction of [**1**-Co(II)Cl]$^{+}$ species and the NO is the [**1**-Co(II)ClNO]$^{+}$ cation reported in the same figure. The calculation of the Fukui function descriptors for this last complex, as well as the oxygen molecule, gives insight on how these species should be approached in order to react. As appears clear from the figure, the reactive site on the complex is located on the nitrogen atom of NO coordinated to the cobalt centre. Following the same reasoning, step by step, it is possible to investigate complicated pathways of reaction with several intermediary steps.

5. Conclusion

The delivery of NO to specific targets has received a great deal of attention due to the important role of NO

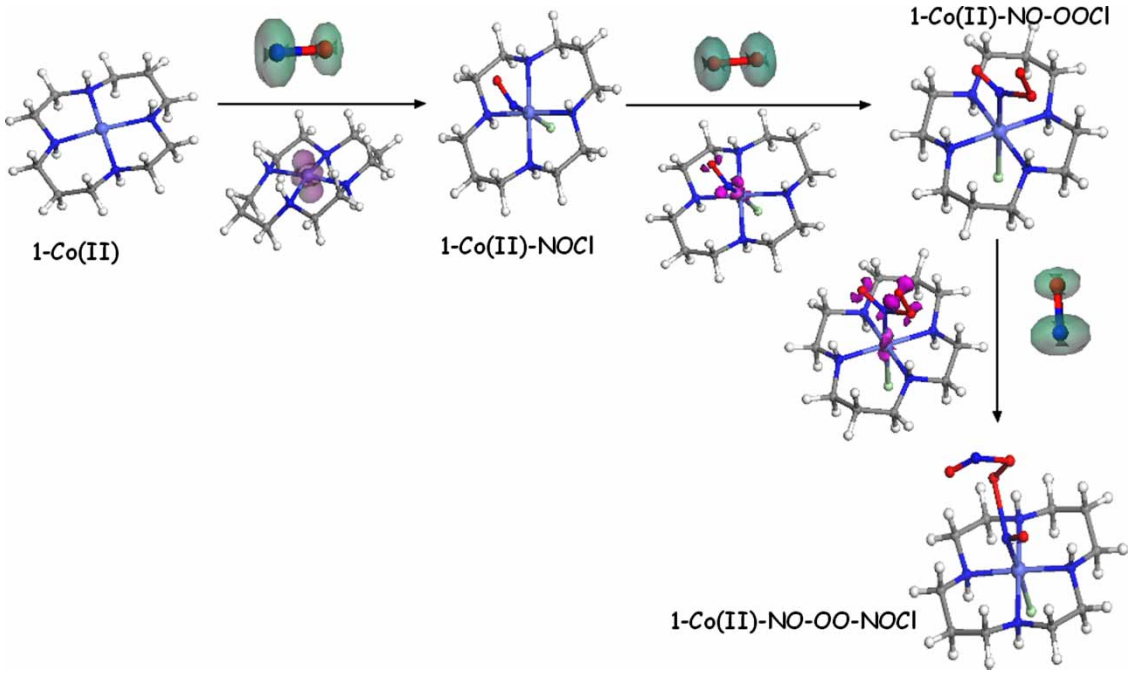

Figure 6. Oxidation scheme for NO catalysed by **1**-Co(II) complex.

in biological systems. Among the possible methods, the use of exogeneous NO gas carried by transition metal complexes has remained poorly explored. We have adopted a combined theoretical–experimental approach in order to determine important parameters that could be used for further tuning the properties of the investigated complex for the target application. The first conclusion of this study is that the solvent effects are extremely important for the realistic description of these complexes and must be taken into account in order to reproduce experimentally observed trends such as the order of relative stabilities of **1**-Co(II) complexes in solutions as well as their reactivity towards the different ligands present in solution. We have predicted that the **1**-Co(II)NO_2NO_2 complex is the most stable one and that it would be possible to observe and isolate it. Moreover, the complex **1**-Co(II)$NONO_2$ turns out to be relatively stable and that it is possible to define experimental conditions in solution to isolate it.

The second conclusion of this work is that calculated vibrational spectra and the Fukui reactivity indices give valuable information on the attribution of the experimental bands and understanding of local reactivity of macrocycle ligands as well as the evolution of reactions involving several steps.

The third conclusion is related to the systematic use of combined theoretical–experimental approaches. We have found that to develop parallel theoretical and experimental investigations is of mutual benefit. More fundamental work on additional, well-characterised transition metal NO-complexes is desirable in order to extend the understanding of the reaction mechanisms and validate the predictive approach to NO controlled release through designing improved macrocycle ligands. One has to recognise that most of the reported studies dealing with the interaction of NO with organometallic and bioinorganic metal complexes have been confronted with the complex redox solution chemistry of NO and obvious experimental difficulties in studying such reactions [48]. Detailed kinetic and mechanistic studies of the autoxidation reactions of bio-inorganic-NO complexes in solution are remarkably scarce. Recent studies have revealed a complex picture in which the coordination of NO becomes associated with drastic changes in the redox nature of the ligand and in the spin state of the metal centre. Important complications that may affect the studies on the interaction of NO with metal centres of macrocycle complexes arise also from the easy oxidation of NO by molecular oxygen in solution to produce NO_2 and N_2O_3 as well as nitrite ions in the presence of an aqueous solution. Computational chemistry when appropriately combined with experiment on these complexes, enhances the understanding of their stability, reactivity and complements the interpretation of observed characterisations as for example the IR vibrational, NMR or EPR spectra.

References

[1] L.J. Ignarro (ed.), *Nitric Oxide: Biology and Pathobiology*, Academic Press, New York, 2000.

[2] P.G. Wang, T.B. Cai, and N. Taniguchi, *Nitric Oxide Donors*, Wiley-VCH, Weinheim, 2005.

[3] R. Rossaint, K.J. Falke, F. Lopez, K. Slama, U. Pison, and W.M. Zapol, *Inhaled nitric oxide for the adult respiratory distress syndrome*, N. Engl. J. Med. 328 (1993), pp. 399–405.

[4] M. Haj Reem, J.E. Cinco, and C.D. Mazer, *Treatment of pulmonary hypertension with selective pulmonary vasodilators*, Curr. Opin. Anaesthesiol. 19 (2006), pp. 88–95.

[5] K. Sydow, A. Daiber, M. Oelze, Z. Chen, M. August, M. Wendt, V. Ullrich, A. Muelsch, E. Schulz, J.F. Keaney, Jr. et al., *Central role of mitochondrial aldehyde dehydrogenase and reactive oxygen species in nitroglycerin tolerance and cross-tolerance*, J. Clin. Invest. 113 (2004), pp. 482–489.

[6] A. Daiber, A. Muelsch, U. Hink, H. Mollnau, A. Warnholtz, M. Oelze, and T. Muenzel, *The oxidative stress concept of nitrate tolerance and the antioxidant properties of hydralazine*, Am. J. Cardiol. 96 (2005), pp. 25i–36i.

[7] J.D. Parker, *Nitrate tolerance, oxidative stress, and mitochondrial function: Another worrisome chapter on the effects of organic nitrates*, J. Clin. Invest. 113 (2004), pp. 352–354.

[8] O.R. Leeuwenkamp, W.P. Van Bennekom, E.J. Van der Mark, and A. Bult, *Nitroprusside, antihypertensive drug and analytical reagent. Review of (photo)stability, pharmacology and analytical properties*, Pharm. Weekbl. Sci. 6 (1984), pp. 129–140.

[9] V. Schulz, *Clinical pharmacokinetics of nitroprusside, cyanide, thiosulfate and thiocyanate*, Clin. Pharmacokinet. 9 (1984), pp. 239–251.

[10] M. Halpenny Genevieve, M. Olmstead Marilyn, and K. Mascharak Pradip, *Incorporation of a designed ruthenium nitrosyl in PolyHEMA hydrogel and light-activated delivery of NO to myoglobin*, Inorg. Chem. 46 (2007), pp. 6601–6606.

[11] A. Franke, F. Roncaroli, and R. van Eldik, *Mechanistic studies on the activation of NO by iron and cobalt complexes*, Eur. J. Inorg. Chem. (2007), pp. 773–798.

[12] C.-Y. Chiang and M.Y. Darensbourg, *Iron nitrosyl complexes as models for biological nitric oxide transfer reagents*, J. Biol. Inorg. Chem. 11 (2006), pp. 359–370.

[13] S.R. Wecksler, A. Mikhailovsky, D. Korystov, and P.C. Ford, *A two-photon antenna for photochemical delivery of nitric oxide from a water-soluble, dye-derivatized iron nitrosyl complex using NIR light*, J. Am. Chem. Soc. 128 (2006), pp. 3831–3837.

[14] P.C. Ford and S. Wecksler, *Photochemical reactions leading to NO and NO_x generation*, Coord. Chem. Rev. 249 (2005), pp. 1382–1395.

[15] A. Eroy-Reveles Aura, Y. Leung, and K. Mascharak Pradip, *Release of nitric oxide from a sol-gel hybrid material containing a photoactive manganese nitrosyl upon illumination with visible light*, J. Am. Chem. Soc. 128 (2006), pp. 7166–7167.

[16] K.E. Broderick, L. Alvarez, M. Balasubramanian, D.D. Belke, A. Makino, A. Chan, V.L. Woods, Jr., W.H. Dillmann, V.S. Sharma, R.B. Pilz et al., *Nitrosyl-cobinamide, a new and direct nitric oxide-releasing drug effective* in vivo, Exp. Biol. Med. 232 (2007), pp. 1432–1440.

[17] J.T. Mitchell-Koch, K.M. Padden, and A.S. Borovik, *Modification of immobilized metal complexes toward the design and synthesis of functional materials for nitric oxide delivery*, J. Polym. Sci. Part A: Polym. Chem. 44 (2006), pp. 2282–2292.

[18] O. Siri, A. Tabard, P. Pullumbi, and R. Guilard, *Iron complexes acting as nitric oxide carriers*, Inorg. Chim. Acta 350 (2003), pp. 633–640.

[19] R.M. Izatt, K. Pawlak, J.S. Bradshaw, and R.L. Bruening, *Thermodynamic and kinetic data for macrocycle interaction with cations, anions, and neutral molecules*, Chem. Rev. 95 (1995), pp. 2529–2586.

[20] R. Ivanikova, I. Svoboda, H. Fuess, and A. Maslejova, *Trans-dichloro(1,4,8,11-tetraazacyclotetradecane)cobalt(III) chloride*, Acta Crystallogr. E Struct. Rep. Online E62 (2006), pp. m1553–m1554.

[21] M.E. Sosa-Torres and R.A. Toscano, *Trans-dichloro(1,4,8,11-tetraazacyclotetradecane)cobalt(III) chloride tetrahydrate 0.47-hydrochloride*, Acta Crystallogr. C C53 (1997), pp. 1585–1588.
[22] J.A. McCleverty, *Reactions of nitric oxide coordinated to transition metals*, Chem. Rev. (Washington, DC) 79 (1979), pp. 53–76.
[23] K. Nakamoto, *Infrared and Raman Spectra of Inorganic and Coordination Compounds*, 3rd ed., Wiley-VCH, New York, 1978.
[24] C.K. Poon, *Infrared spectra of some* cis- *and* trans-*isomers of octahedral cobalt(III) complexes with a cyclic quadridentate secondary amine*, Inorg. Chim. Acta 5 (1971), pp. 322–324.
[25] J.A. McCleverty, *Chemistry of nitric oxide relevant to biology*, Chem. Rev. (Washington, DC) 104 (2004), pp. 403–418.
[26] B. Delley, *An all-electron numerical method for solving the local density functional for polyatomic molecules*, J. Chem. Phys. 92 (1990), pp. 508–517.
[27] B. Delley, *From molecules to solids with the Dmol^3 approach*, J. Chem. Phys. 113 (2000), pp. 7756–7764.
[28] B. Delley, *The conductor-like screening model for polymers and surfaces*, Mol. Simul. 32 (2006), pp. 117–123.
[29] A. Klamt and G. Schueuermann, *COSMO: A new approach to dielectric screening in solvents with explicit expressions for the screening energy and its gradient*, J. Chem. Soc. Perkin Trans. II (1993), pp. 799–805.
[30] J. Andzelm, C. Kolmel, and A. Klamt, *Incorporation of solvent effects into density functional calculations of molecular energies and geometries*, J. Chem. Phys. 103 (1995), pp. 9312–9320.
[31] J.J.P. Stewart, *Optimization of parameters for semiempirical methods. I. Method*, J. Comput. Chem. 10 (1989), pp. 209–220.
[32] J.J.P. Stewart, *Optimization of parameters for semiempirical methods. II. Applications*, J. Comput. Chem. 10 (1989), pp. 221–264.
[33] *Spartan O2 Wavefunction, Inc.*, Irvin, CA (2002).
[34] *Cs Chem3d 10.0 CambridgeSoft*, Cambridge, MA (2006).
[35] K. Fukui, *Reactivity and Structure Concepts in Organic Chemistry, Vol. 2: Theory of Orientation and Stereoselection*, Springer-Verlag, New York, 1975.
[36] R. Franke, *Theoretical Drug Design Methods*, Amsterdam, Elsevier, 1984.
[37] D.F.V. Lewis, C. Ioannides, and D.V. Parke, *Interaction of a series of nitriles with the alcohol-inducible isoform of P450: Computer analysis of structure–activity relationships*, Xenobiotica 24 (1994), pp. 401–408.
[38] Z. Zhou and R.G. Parr, *Activation hardness: New index for describing the orientation of electrophilic aromatic substitution*, J. Am. Chem. Soc. 112 (1990), pp. 5720–5724.
[39] R.G. Pearson, *Hard and soft acids and bases*, J. Am. Chem. Soc. 85 (1963), pp. 3533–3539.
[40] R.G. Pearson, *Acids and bases*, Science (Washington, DC) 151 (1966), pp. 1721–1727.
[41] R.G. Pearson, *Absolute electronegativity and hardness correlated with molecular orbital theory*, Proceedings of the National Academy of Sciences of the United States of America 83 (1986), pp. 8440–8441.
[42] R.G. Pearson and J. Songstad, *Application of the principle of hard and soft acids and bases to organic chemistry*, J. Am. Chem. Soc. 89 (1967), pp. 1827–1836.
[43] R.G. Parr and P.K. Chattaraj, *Principle of maximum hardness*, J. Am. Chem. Soc. 113 (1991), pp. 1854–1855.
[44] R.G. Parr and J.L. Gazquez, *Hardness functional*, J. Phys. Chem. 97 (1993), pp. 3939–3940.
[45] R.G. Parr and R.G. Pearson, *Absolute hardness: Companion parameter to absolute electronegativity*, J. Am. Chem. Soc. 105 (1983), pp. 7512–7516.
[46] M.L. McKee, Ab initio *Study of the N_2O_4 potential energy surface. Computational evidence for a new N_2O_4 isomer*, J. Am. Chem. Soc. 117 (1995), pp. 1629–1637.
[47] L.P. Olson, K.T. Kuwata, M.D. Bartberger, and K.N. Houk, *Conformation-dependent state selectivity in O—O cleavage of ONOONO: An "Inorganic Cope Rearrangement" helps explain the observed negative activation energy in the oxidation of nitric oxide by dioxygen*, J. Am. Chem. Soc. 124 (2002), pp. 9469–9475.
[48] M. Feelisch and J.S. Stamler (eds), *Methods in Nitric Oxide Research*, John Wiley & Sons Inc., New York, 1996.